Version of record at: https://doi.org/10.1149/1945-7111/ac7adf

Journal of The Electrochemical Society, 2022 **169** 073503

Hydrogen-powered Electrochemically-driven CO_2 Removal from Air Containing 400 to 5000 ppm CO_2

Stephanie Matz,* Lin Shi, Yun Zhao, Shimshon Gottesfeld, Brian P. Setzler,**,z and Yushan Yan**,z**

Department of Chemical and Biomolecular Engineering, University of Delaware, Newark, Delaware 19716, United States of America

The performance of a hydrogen-powered, electrochemically-driven CO_2 separator (EDCS) was demonstrated at cathode inlet CO_2 concentrations from 400 ppm to 5,000 ppm. The impact of current density and CO_2 concentration were evaluated to predict operating windows for various applications. The single-cell data was used to scale a 100 cm^2, multi-cell stack using a shorted-membrane design for four applications: direct air capture (DAC), hydroxide exchange membrane fuel cell (HEMFC) air pretreatment, submarine life support, and space habitation. For DAC, a 339-cell EDCS stack (7.7 L, 17 kg) was projected to remove 1 tonne CO_2 per year. The addition of the EDCS in HEMFC systems would result in nearly a 30% increase in volume, and therefore further improvements in performance would be necessary. A module containing five 338-cell EDCS stacks (38 L, 85 kg) in parallel can support a 150 person crew at 2.1% of the volume of the liquid amine system employed in submarines. For space habitation, a 109-cell EDCS stack (3.2 L, 10 kg) is adequate for 6 crewmembers, and is less than 1% the size and 5% the weight of the current CO_2 removal system installed on the International Space Station.

Manuscript submitted March 21, 2022; revised manuscript received June 10, 2022. Published July 7, 2022. *This paper is part of the JES Focus Issue on Electrochemical Separations and Sustainability.*

Supplementary material for this article is available online

Carbon capture has been lauded as a promising area of research. Rapid economic growth and the corresponding increase in use of fossil fuels has resulted in a rise in the atmospheric carbon dioxide (CO_2) levels from 304 ppm[1] to 417 ppm[2] in the last century. The rise in anthropogenic greenhouse gas emissions (GHG) have been linked to global warming and climate change which has spurred research to capture CO_2. A bulk of this research has focused on CO_2 capture at point sources where CO_2 concentrations are high making separations more favorable and efficient. However, there is an increasing interest in CO_2 removal technologies focused on low CO_2 concentrations, defined here as below 0.5% CO_2.[3–10] Areas that will benefit from the development of these low CO_2 concentration technologies include: direct air capture (DAC), air compression pretreatment for medical or SCUBA use,[5] air-breathing hydroxide exchange membrane fuel cell (HEMFC) pretreatment,[11,12] building[13] and mining ventilation, nuclear submarine life support systems, and space habitation.[5] State-of-the-art technologies for these applications primarily involve solvent absorption and solid adsorption. For long-term continuous operation, both types of technologies rely on a supply of fresh sorption material or additional equipment and energy for regeneration.[5,14] These limitations are especially prevalent in transport and life support applications where supplies are not readily available and volume/weight are constrained.[15–17] Recently, there has been more interest in electrochemical separation of CO_2 which has the potential to allow for continuous CO_2 removal at low concentrations while meeting strict volume/weight requirements.

The electrochemically-driven CO_2 separator (EDCS) is a promising and versatile CO_2 removal technology that takes advantage of the alkaline environment of an anion exchange membrane to scrub CO_2 from air.[11,12,18] The EDCS operates similarly to a HEMFC: oxygen in air fed to the cathode undergoes the oxygen reduction reaction (ORR) while hydrogen fed to the anode undergoes the hydrogen oxidation reaction (HOR).

$$\textit{Cathode}: \frac{1}{2}O_2 + H_2O + 2e^- \rightarrow 2OH^- \quad [1]$$

$$\textit{Anode}: 2OH^- + H_2 \rightarrow 2H_2O + 2e^- \quad [2]$$

However, the EDCS is operated to maximize CO_2 separation, ignoring power generation. In order to achieve this, the EDCS is operated at high air flows to maximize CO_2 capture at the cathode, but maintain low hydrogen feed flow and low current densities in order to maximize electron efficiency for CO_2 separation. Hydroxide anions generated by the cell current at the EDCS cathode effectively capture CO_2 from air even at low, sub-ambient concentrations via the following processes:

$$CO_2 + H_2O \rightleftharpoons H_2CO_3 \quad [3]$$

$$CO_2 + OH^- \rightleftharpoons HCO_3^- \quad [4]$$

$$H_2CO_3 \rightleftharpoons HCO_3^- + H^+ \quad [5]$$

$$HCO_3^- \rightleftharpoons CO_3^{2-} + H^+ \quad [6]$$

The kinetics of Eqs. 3 and 4 determine the rate of CO_2 capture in the EDCS at a given cell current while Eqs. 5 and 6 are fast and always equilibrated.[19] It is important to note that CO_2 is not directly involved in the electrochemical reactions. Cell current controls the rate of hydroxide generated at the cathode, and hydroxide participates in the CO_2 hydration reaction when CO_2 is present in the air stream. As such, a carbon-ionomer cathode interlayer was introduced to the EDCS in Matz et al. (2021)[11] between the cathode catalyst layer and anion exchange membrane as seen in Fig. 1. The electrochemical reaction that generates hydroxide occurs exclusively within the catalytically-active cathode catalyst layer with the potential driving the ions toward the anode. Thus, the interlayer is a hydroxide-rich volume of space where CO_2 gas can penetrate from the flow fields and react with hydroxide. Carbonate and bicarbonate anions formed at the cathode and interlayer are transported across the membrane to the anode due to the potential gradient created by the concurrent HOR and ORR reactions. Carbonates build up in the

*Electrochemical Society Student Member.
**Electrochemical Society Member.
zE-mail: setzler@udel.edu; yanys@udel.edu

Version of record at: https://doi.org/10.1149/1945-7111/ac7adf

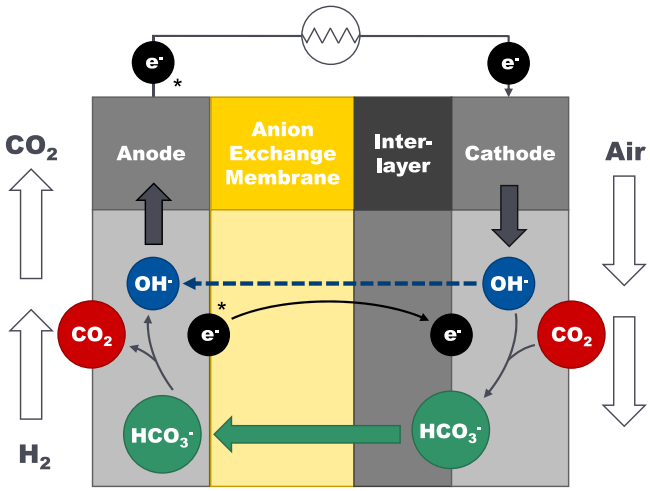

Figure 1. Simplified diagram of EDCS of cell components, relevant species in each layer, and species flow paths. The interlayer is a carbon-ionomer layer between the cathode and anion exchange membrane (AEM). There are two methods shown to complete the electronic circuit indicated by *. An external circuit can be completed by an external wire connecting the anode to the cathode. An internal circuit can be completed by the introduction of a carbon-composite AEM, allowing for direct transport of electrons from the anode to the cathode through the membrane and interlayer.

anode, decreasing the local pH, and thereby promoting the release of CO_2.[20,21] This yields a concentrated CO_2 product stream at the anode with only water as the byproduct. Once again, CO_2 is not directly involved in the electrochemical reaction. As CO_2 is released as a gas into the anode stream, hydroxide ions are formed. Water is then generated by the subsequent HOR reaction between hydroxide and hydrogen, freeing electrons which are then transported back to the cathode. Unlike sorption-based technologies, the EDCS continuously self-regenerates electrochemically as ORR ensures a constant supply of hydroxide for CO_2 capture at the cathode, and CO_2 is continually released at the anode following sufficient carbonate buildup.

Typically, in fuel cells, the electronic circuit is completed by conducting electrons from the anode to cathode via an external circuit, producing power. Since power production is not the goal of the EDCS, an external circuit is not required. By using a carbon-composite anion exchange membrane (or "shorted membrane") like the one discussed in Shi et al. (2022),[12] an internal circuit can be established, allowing electrons to flow directly from the anode to the cathode. Both of these electron pathways are in the EDCS schematic shown in Fig. 1. The introduction of an internal circuit removes the need for bipolar plates and can greatly reduce the size of the final device. However, when using the shorted membrane, cell current cannot be directly controlled, requiring the development of alternative control schemes to indirectly control current via hydrogen flow and limiting current at the anode.[11,12] Similar or better CO_2 removal performance has been achieved using the shorted membranes as the standard membranes described above.[12]

Others have observed the phenomena of CO_2 scrubbing in alkaline electrochemical devices. Wynveen et al. (1972)[22] and Winnick et al. (1974)[23] initially developed hydrogen-powered, chemical-electrochemical devices using alkaline electrolytes for CO_2 removal in life support applications. Numerous researchers have noted the sensitivity of HEMFCs to the presence of CO_2 in air and subsequent CO_2 purging mechanism at the anode, resulting in a substantial voltage loss and decreased power production.[20,21,24–33] Similarly, the transport of (bi)carbonates across the membrane has been shown to have a negative impact in CO_2 electrolysis when using an anion exchange membrane, resulting in a loss of reactant.[34–37] But the focus of most of these works has been on mitigating the impact or limiting transport of CO_2 not improving CO_2 separation with the exception of Zheng et al. (2021).[18] Additionally, technologies reliant on applied voltage, such as electrodialysis[9,38,39] or oxygen pump,[40–45] have been proposed for CO_2 separation and concentration. Recently, there has been some interest in coupling CO_2 separation and concentration with a H_2-air electrochemical cell using an anion exchange membrane.[11,12,18,46] No other research to the author's knowledge has focused on optimizing the hydrogen-power, electrochemically-driven CO_2 separation for the range of CO_2 concentrations focused in this work or the range of applications under consideration.

Of the numerous applications in need of advancements in CO_2 removal technologies, four are of particular interest for use of the EDCS: (i) direct air capture (DAC), (ii) treatment of air feed upstream of the HEMFC stack, (iii) nuclear submarine life support systems, and (iv) manned-spacecraft air revitalization.

(i) *Direct air capture*: In order to reduce GHG in the atmosphere and meet climate mitigation goals, a broader CO_2 capture approach must be implemented including direct air capture. DAC is a relatively new strategy requiring significant advancements in CO_2 removal technologies to efficiently and cost-effectively remove CO_2 from air at ambient levels and at rates that will impact the global atmospheric concentration of CO_2.[3,6]

(ii) *Treatment of air feed to HEMFC stacks*: A hydroxide exchange membrane fuel cell stack operating on ambient air is an attractive alternative to the proton exchange membrane fuel cell (PEMFC) stack that currently dominates the fuel cell vehicle market. HEMFCs have the potential to reduce costs compared to the PEMFC because the alkaline environment allows for the use of non-platinum group metal catalysts and cheaper construction materials.[47] However, HEMFCs are highly vulnerable to CO_2 at atmospheric concentrations as carbonation is associated with significant loss of power.[20,21,25,26,29,31,33,48–54] In order to achieve performance parity with the incumbent PEMFC, CO_2 must be removed from the air feed stream prior to the HEMFC stack. This requires a technology to remove CO_2 continuously and efficiently from air down to single digit ppm levels within a compact, lightweight, and low-cost device.

(iii) *Nuclear submarine life support*: The life support systems in nuclear submarines are responsible for ensuring a healthy, breathable atmosphere for the crew. The life support system includes oxygen generation, removal of particulates and odors, and CO_2 separation.[16,55] Each crewmember aboard the submarine consumes 0.90 kg_{O_2} day^{-1} [55,56] which must be supplied by the oxygen generation system. In submarines, oxygen is produced by sending desalinated seawater to a water electrolyzer, producing a hydrogen byproduct. Oxygen is sent to the cabin air while hydrogen is vented overboard to prevent accumulation. Meanwhile, cabin air is recirculated over electrostatic filters and activated carbon beds to remove particulates and odors, respectively.[55] In addition to particulates and odors, each crewmember aboard the submarine generates 1.04 kg_{CO_2} day^{-1} [56] which must be removed then vented overboard. The separation of CO_2 from cabin air is a vital process for ensuring the health and safety of the crew and prolonging the ability of the submarine to remain submerged. Currently, liquid amine systems (LAS) using monoethanolamine as a solvent are used to remove CO_2 produced by the crew from the cabin air.[16,17,57] The liquid amine system is bulky and complex as the amine solvent must be regenerated via pressure and thermal desorption of the CO_2 to maintain continuous operation.[58] Submarine life support systems have historically operated at nearly 5,000 ppm CO_2 which is a relatively high CO_2 concentration for human occupancy.[16] This is in part due to the constraints of the CO_2 removal technology efficiency and space available within the confines of the submarine.[17] Prolonged exposure to high CO_2 concentrations has been

linked with numerous health issues and decreased cognition.[59] In light of this, the Navy is looking to reduce the cabin air CO_2 concentration to below 3,000 ppm to ensure the health and safety of the crew during extended submersions.[17] Improvements in efficiency and compactness of the CO_2 removal technology is needed to attain this more stringent requirement.

(iv) *Manned-spacecraft air revitalization*: Space habitation systems require air revitalization for prolonged, manned space travel. Unlike the submarine life support systems, space-based life support systems are nearly closed-loop as resupply is not feasible during extended missions.[60] The life support system includes oxygen generation, CO_2 removal, particulate and odor removal, and water recovery. Water and oxygen are valuable resources and must be recycled within the life support system. Cabin oxygen is replenished via water electrolysis using the limited water supply or recycled water recovered from human respiration.[61] Hydrogen is produced as a byproduct of water electrolysis, and its use is dependent on whether the air revitalization system is open- or closed-loop. In a closed-loop life support system, CO_2 captured from cabin air and hydrogen from the water electrolyzer are fed to a Sabatier reactor to produce methane and water. The water is then recovered and recycled back into the life support system.[62] In open-loop life support systems, CO_2 and hydrogen are vented into space. CO_2 is removed from cabin air using sorbent-based technologies to counteract crew respiration rates and to maintain levels below 3,300 ppm.[61] NASA is looking to further reduce the cabin air CO_2 concentration to less than 2,600 ppm as more research of the negative health and cognitive impacts of CO_2 on the crew becomes available[63] and NASA considers extending mission durations.[62] Typical CO_2 removal technologies such as amines and solid adsorbents struggle to meet the CO_2 removal targets at the tight volume and weight requirements for space travel. The Carbon Dioxide Removal Assembly (CDRA) on the International Space Station (ISS) uses a solid adsorbent technology to remove CO_2; however, this technology cannot meet the reduced target CO_2 concentrations as designed[63] and has been plagued with maintenance issues due to particulate leakage during its tenure on the ISS.[15,64]

The EDCS is a promising CO_2 removal technology for use in these four applications. The EDCS is able to effectively remove CO_2 from an air stream at sub-ambient levels using a small hydrogen stream to power the separation. In DAC, a green hydrogen source must be supplied for net negative CO_2 emissions to be achieved, possibly by the addition of water electrolyzers powered by renewable energy. In the other applications, existing hydrogen waste streams can be utilized such as the stack purge in the HEMFC vehicle and the hydrogen byproduct from water electrolysis in both life support systems. In life support applications, it is important to note that the EDCS consumes both hydrogen and oxygen, and thus the water electrolysis unit will need to be sized accordingly. Although the EDCS will require a larger electrolyzer, it is able to utilize the existing system and removes the need for regeneration and its associated equipment. As the EDCS is a membrane technology, we are able to efficiently package large areas into small volumes using configurations such as plate-frame stacks or spiral wound modules which allows for high air processing without large increases in volume.[12,65]

The main focus of the ensuing paper is to demonstrate EDCS performance in CO_2 removal from air streams at moderate CO_2 levels ranging from 400 ppm to 5,000 ppm, which are relevant to the applications discussed above. Additionally, we investigate some key parameters requiring optimization to achieve minimal outlet CO_2 concentrations and hydrogen consumption at the highest viable air throughput. Single-cell testing focused on the performance using the standard AEM to allow the current to be directly measured and controlled. This allowed the hydrogen consumption to be directly measured and removed confounding factors associated with operation of the shorted-membrane EDCS over a wide operating window. It should be noted that the shorted-membrane EDCS performance has been demonstrated to be comparable to the standard AEM by Shi et al. (2022).[12] After determining the performance of the EDCS at relevant operating conditions, a scaled EDCS stack module is proposed and compared to incumbent technologies to assess its feasibility.

Table I. Ink recipes used for preparation of MEAs.

	Electrodes	Interlayer
Catalyst/Carbon (mg)	12.5 (Pt/C)	25 (Vulcan XC-72)
Deionized water (μL)	50	0
HEI Solution, 3.5 wt% (mg)	89	360
Isopropyl alcohol (mL)	1.25	1.67
Active Area (cm^2)	25	25

Methods

Membrane electrode assembly (MEA) preparation.—MEAs were fabricated using PAP-TP-85 membranes (Versogen, 70 μm), Pt/C catalyst (Alfa Aesar HiSpec 4000, 40 wt% Pt on Vulcan XC-72) at both electrodes, carbon black (Cabot, Vulcan XC-72) in the cathode interlayer, and 3.5 wt% PAP-TP-85 ionomer solutions in ethanol.[66] The electrodes were prepared with an ionomer to carbon (I:C) weight ratio of 0.4 while the cathode interlayer I:C ratio was 0.45. The recipes for the inks are shown in Table I. Prior to hand-spraying, inks were sonicated in an ice bath for 1 h. The anode and interlayer inks were sprayed directly onto the membrane and the cathode ink was sprayed on top of the interlayer ink using an Iwata-Medea airbrush and a 25 cm^2 active area stencil to produce the MEAs.

CO_2 separation testing protocol.—The EDCS cell was assembled with the prepared, 25 cm^2 active area MEAs sandwiched between gaskets and a gas diffusion layer (GDLs) or nickel mesh in single cell hardware from Fuel Cell Technologies, Co. Gasket thickness was adjusted based on the gas diffusion layer (for the anode) or nickel mesh (for the cathode) thickness to ensure it was not overcompressed or damaged the membrane. For SGL 29BC GDL, a 127 μm polytetrafluoroethylene (PTFE) gasket was used in concert with a 13 μm fluorinated ethylene propylene (FEP) subgasket. For the woven nickel mesh (26 threads per inch, 530 μm), two 254 μm thick FEP gaskets were used with a 13 μm FEP subgasket. A Scribner 850e fuel cell test system with a backpressure module was used for testing. Cathode outlet CO_2 concentration was monitored using a Teledyne TML20 CO_2 analyzer (0–2,000 ppm CO_2) or Vaisala GMP252 CO_2 probe (0–5,000 ppm CO_2) preceded by a chilled condenser.

After assembly, a similar break-in procedure as described in Matz et al. (2021)[11] was performed prior to CO_2 removal testing. The cell was heated to 60 °C while flowing oversaturated nitrogen by keeping the cell temperature below the humidifier temperatures. The anode and cathode humidifiers were heated concurrently to 57.7 °C (90% relative humidity). Once temperatures were stabilized, 500 sccm H_2 and 500 sccm O_2 were fed to the anode and cathode, respectively. The cell was activated by increasing the current density in steps then allowing the voltage to stabilize before stepping the current again. An example of the current density steps and voltage response during break-in are shown in **Fig. SI-1.** The cell had similar break-in response as that shown in Shi et al. (2020)[67] where the voltage initially drops as current density steps up and a voltage recovery is observed. Activation was considered complete when voltage stabilized below 0.3 V. After activation, temperatures were adjusted to test conditions and CO_2-containing air was introduced to the cell while maintaining a current density of 20 mA $cm+^2$. The

Version of record at: https://doi.org/10.1149/1945-7111/ac7adf

transient voltage response of an example cell when air containing 400 ppm CO_2 is introduced to the cathode is shown in **Fig. SI-2.** As CO_2 enters the cell, the voltage gradually decreases and stabilizes as a steady-state is reached, following the characteristic curve observed by Zheng et al. (2020).[48]

When testing the EDCS, air containing a range of CO_2 concentrations was fed to the EDCS cathode from a 10% CO_2 air mixture (Keen Compressed Gas Co.) combined with CO_2-free air. The cathode flow was 3000 sccm air containing CO_2, unless specified. Hydrogen was fed at 12 sccm H_2 (unless otherwise stated) to the anode which is slightly higher than the hydrogen consumption rate at 50 mA cm^{-2} (9 sccm H_2). It has been previously demonstrated that hydrogen flow can approach the theoretical stoichiometric limit without significant impact on CO_2 removal performance.[11] Each set of operating conditions was held for 1 h with data collected at 10 s intervals and the latter 30 min-average reported.

Single-Cell EDCS Experimental Results

In order for the EDCS to be considered a feasible CO_2 removal solution for the previously mentioned applications, the EDCS must be able to remove CO_2 effectively at a range of CO_2 feed concentrations and relevant operating temperatures. Figure 2 shows EDCS performance parameters at cathode inlet CO_2 concentrations ranging from 400 ppm to 5,000 ppm at current densities of 10, 20, and 30 mA cm^{-2} and at temperatures of 40 °C and 60 °C.

Increasing inlet CO_2 concentration at a given current density from 400 to 5,000 ppm resulted in an increase in the CO_2 flux but the fraction of CO_2 removed decreased. Higher inlet CO_2 concentrations shifts the acid-base equilibria in Eqs. 3 and 4 towards the right promoting CO_2 capture and resulting in a higher CO_2 flux. At low inlet CO_2 concentrations, there is less overall CO_2 entering the EDCS and therefore, lower CO_2 flux is attained for a given CO_2 removal and current density. This can be shown by the following relationship:

$$N_{CO_2} = \chi \frac{y_{CO_2} \dot{V}_{air}}{A V_{IG}} \quad [7]$$

where N_{CO_2} is the CO_2 flux, χ is the fraction of CO_2 removed, y_{CO_2} is the mole fraction of CO_2 fed to the EDCS, $\dot{V}_{air}$ is the volumetric flow rate of air to the cathode, and V_{IG} is the molar volume. The fraction of CO_2 removed is a function of inlet CO_2 concentration, cathode flow, current density, and gas-phase mass transport in the cathode. At 100% CO_2 removal, where $\chi = 1$, Eq. 7 represents the maximum theoretical CO_2 flux the EDCS could achieve based on the inlet CO_2 concentration and air flow rate. Higher CO_2 flux reduces the required active area and/or the processed air flow in order to achieve the same CO_2 removal rate. This is important when evaluating the EDCS for life support applications where size and weight constrain the system.

The cell current is the main user controlled parameter of the EDCS. Current density influences the rate of hydroxide generation at the cathode catalyst layer as well as the rate of ionic flux, including hydroxide and (bi)carbonate ions, across the membrane. Current density, $\frac{I}{A}$, can be related to the CO_2 flux by

$$N_{CO_2} = \frac{I}{\mathrm{nFA}} \quad [8]$$

where I is the current, n is number electrons transferred per CO_2, F is Faraday's constant, and A is the active area. For the case of

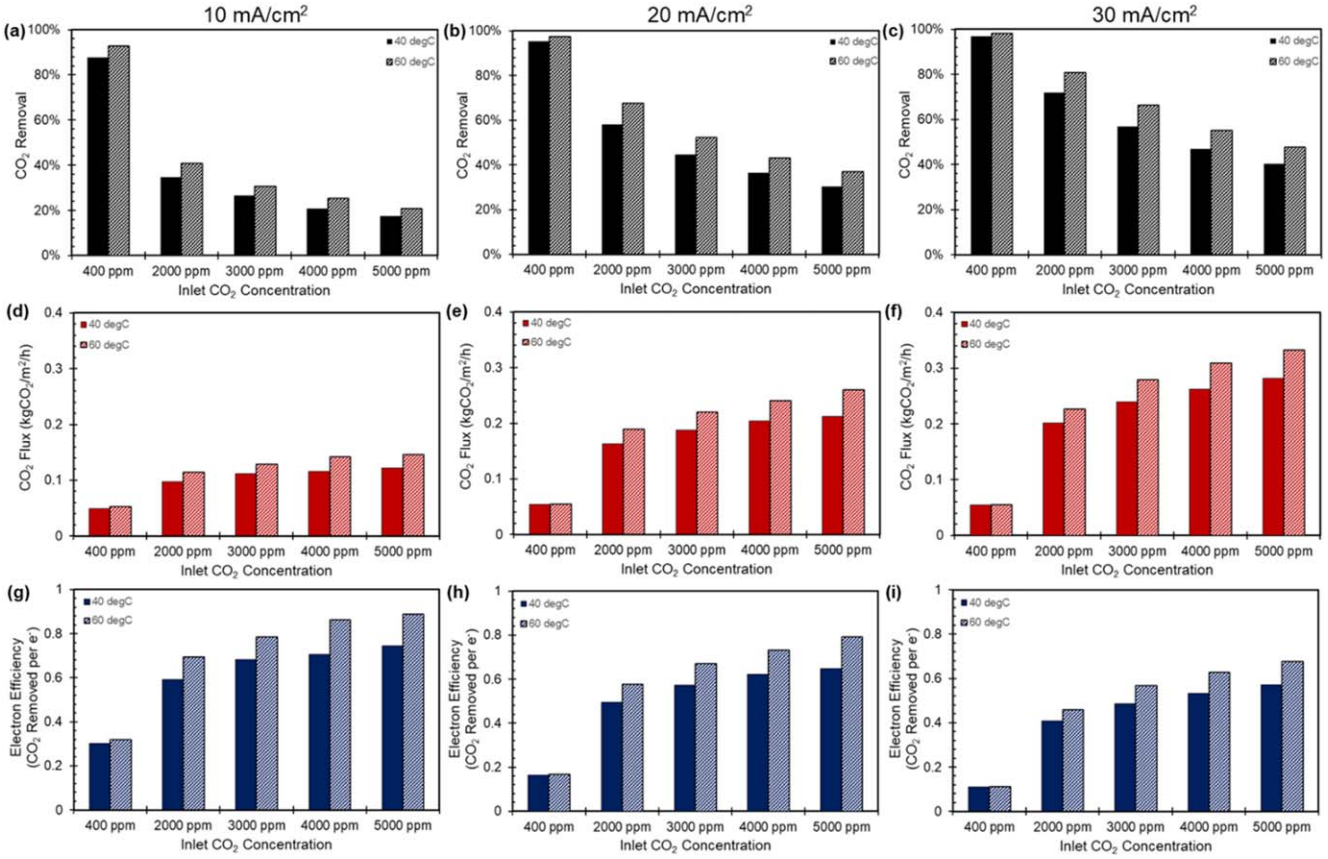

Figure 2. EDCS performance for a range of cathode inlet CO_2 concentrations: (a-c) show the percentage of carbon dioxide removed, (d-f) show carbon dioxide flux across the cell, and (g-i) show electron efficiency which defines hydrogen consumption. From left to right, the columns show EDCS performance at 10, 20, and 30 mA cm^{-2}. All tests were performed at 40 °C or 60 °C (70% RH) operating with an anode flow of 12 sccm H_2 and cathode flow of 3000 sccm air with the reported CO_2 concentrations. Backpressure was 0 kPa(g) on both the anode and the cathode.

Version of record at: https://doi.org/10.1149/1945-7111/ac7adf

100% electron efficiency, n is assumed to be equal to one electron transferred per CO_2 based on the bicarbonate stoichiometry shown in Eq. 4 and electron efficiency is defined as the inverse, $1/n$. As current density increased from left to right across Fig. 2, both the fraction of CO_2 removed and the CO_2 flux increased as more hydroxide ions were generated at the cathode catalyst layer increasing the rate of CO_2 capture and ionic flux across the membrane. The improvement in CO_2 removal is more easily observed at cathode inlet CO_2 concentrations above 2,000 ppm. At 400 ppm, the fraction of CO_2 removed is nearing 100% even at 10 mA cm^{-2}, and hence there is very little room for fraction of CO_2 removed or CO_2 flux to improve. But increasing current density resulted in lower electron efficiency, indicating not all hydroxide was converted to bicarbonate due to mass transport, kinetic, and/or thermodynamic limitations in the system. Whereas increasing inlet CO_2 concentration at a given current density increased electron efficiency. More CO_2 entering at constant rate of hydroxide generation results in more CO_2 molecules captured and transferred per hydroxide ion. Electron efficiency is inversely related to the hydrogen consumption, and a valuable parameter to assess the EDCS energy efficiency compared to other CO_2 removal technologies. Higher electron efficiency means lower hydrogen consumption and lower energy costs to separate CO_2. For certain applications at low CO_2 concentrations, electron efficiency will be the most important EDCS performance parameter for determining economics (such as DAC), and thus even lower current densities will need to be investigated to improve electron efficiency.

Figure 3 compares the EDCS CO_2 flux at 400 ppm for a range of current densities against the ideal CO_2 fluxes defined by Eqs. 7 and 8 Ideal performance of the EDCS with 100% electron efficiency and 100% CO_2 removal is represented by the intersection of the black and red lines, which is 3.5 mA cm^{-2} for this set of conditions. Experimental performance falls below these thresholds due to non-idealities in the EDCS. Increasing current density results in a sharp rise in CO_2 flux before it plateaus. By 20 mA cm^{-2}, the experimental CO_2 flux is nearly at the limit set by 100% CO_2 removal; therefore, increasing current density beyond this range results in a reduction in electron efficiency due to excess hydroxide generation without any improvement in CO_2 capture because the system is limited by the rate at which CO_2 enters the EDCS. Based on this data, the operating current density for DAC and air pretreatment upstream of a HEMFC stack will be quite different. In DAC where the goal is to cheaply capture CO_2, electron efficiency and therefore hydrogen consumption will be the determining factor for choosing the current density. In order to minimize hydrogen consumption and the associated cost, a low current density near the intersection of the black and red line should be chosen. Operation in this regime balances the competing demands of maximizing CO_2 removal to reduce air throughput and minimizing excess hydroxide generation to avoid "wasted" electrons. In Fig. 3b, the electron efficiency peaks near 5 mA cm^{-2}. Insufficient current density can result in poor electron efficiency due to bicarbonate back-diffusion from the anode as a result of the (bi) carbonate concentration profiles. For the HEMFC vehicle application, high CO_2 removal greater than 99% is the determining factor, and therefore a higher operating current density must be chosen at a penalty to electron efficiency. However, it should be noted that the influx of CO_2 at 400 ppm is relative small and would not require large hydrogen flows relative to the air processed even at low electron efficiencies of 5%–0% (5–10 H_2 per CO_2 removed). For each CO_2 removal application, there will be tradeoffs for the operating parameters chosen on the EDCS CO_2 removal performance.

Figure 2 also shows the impact of increasing the operating temperature from 40 °C to 60 °C on the EDCS performance parameters. Increasing temperature improved all three parameters: CO_2 removal, CO_2 flux, and electron efficiency. The improved performance at higher temperatures is primarily a result of the faster kinetics associated with the chemical reaction between hydroxide and carbon dioxide (Eq. 4). The actual operating temperature of the EDCS will depend on the constraints of the application. HEMFC vehicles are projected to operate at 80 °C or more, but in DAC and life support systems, the EDCS will need to operate at levels closer to ambient. Minimizing extraneous equipment such as heat exchangers will be vital for reducing the capital cost in DAC and the size and weight of the system in life support systems. Finally, it is important to note that the operating temperature range of the EDCS is mild compared to other CO_2 removal technologies like those based on sorbents or cryogenics, giving the EDCS an important advantage.

A subset of EDCS performance at varying cathode flows and inlet CO_2 concentrations is shown in Fig. 4. Similar to increasing inlet CO_2 concentration, as cathode flow increases, the percentage of CO_2 removed decreases while CO_2 flux and electron efficiency increase. Increasing the air flow rate increases the amount of CO_2 entering the EDCS in a given time, resulting in a lower single pass CO_2 removal but allowing for a higher CO_2 flux. As hydroxide generation rate is determined by the set current density, the amount of hydroxide available does not change at a given current density. Therefore, as CO_2 flux increases, the electron efficiency increases at a given current density. Higher air flow rates which will be required life support systems due to strict volume constraints and will result

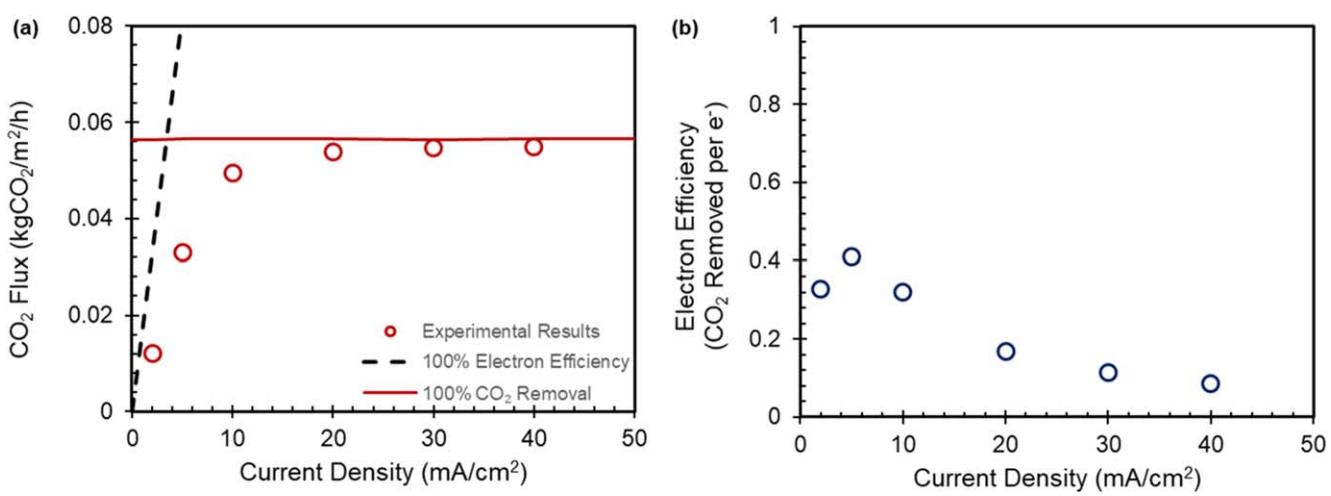

Figure 3. EDCS (a) CO_2 flux and (b) electron efficiency measured for a range current densities when fed air with 400 ppm CO_2. The black dashed line represents theoretical flux at 100% electron efficiency (see Eq. 8) and the red solid line represents theoretical flux at 100% CO_2 removal (see Eq. 7). All tests were performed at 40 °C (70% RH) operating with an anode flow of 12 sccm H_2 and cathode flow of 3000 sccm air containing 400 ppm CO_2. Backpressure was 0 kPa(g) on both the anode and the cathode.

Version of record at: https://doi.org/10.1149/1945-7111/ac7adf

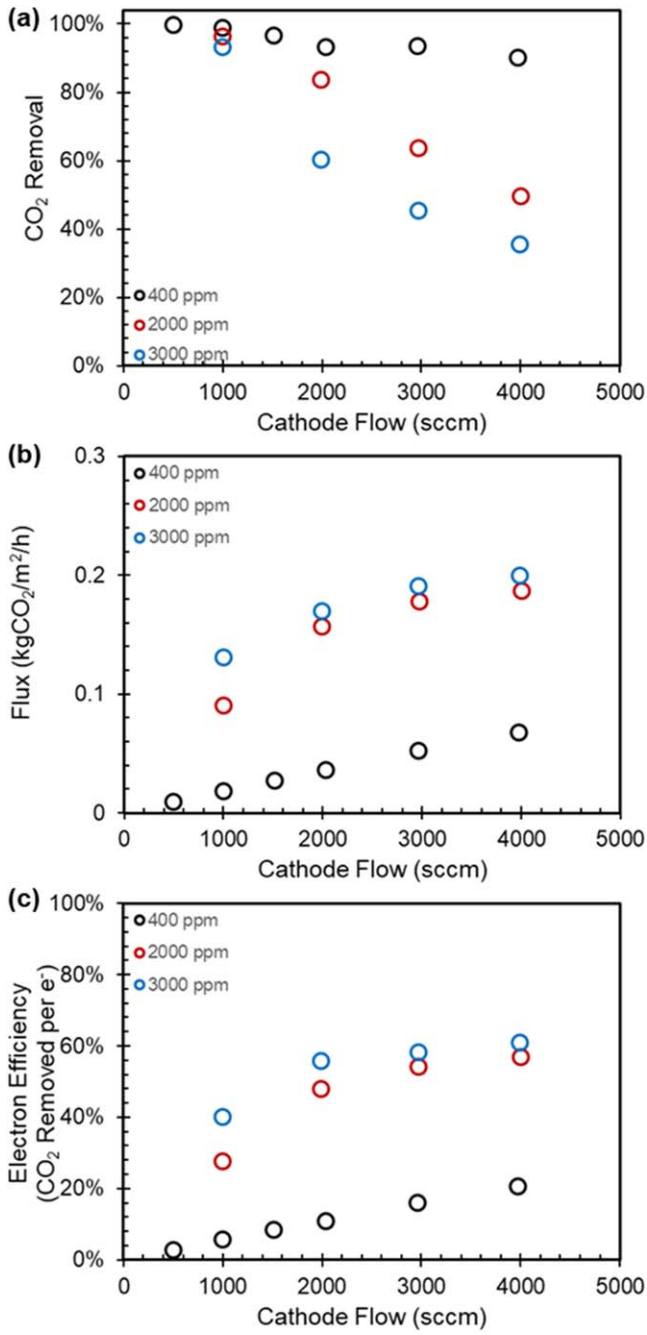

Figure 4. EDCS performance measured for a range of cathode flow rates when fed air with CO_2 concentrations of 400, 2,000, and 3,000 ppm: (a) shows percentage of carbon dioxide removed, (b) shows carbon dioxide flux, and (c) shows electron efficiency. All tests were performed at 60 °C (70% RH) operating at a current density of 20 mA cm^{-2} with an anode flow of 12 sccm H_2 and a cathode flow of air containing CO_2. Backpressure was 0 kPa (g) on both the anode and the cathode.

in higher pressure drops in the EDCS. Therefore, there will be higher fan/blower energy consumption which will in turn effect the cost of CO_2 separation. Reduced air flows increase CO_2 removal but require increased active area and therefore, increase capital cost. As such, the cathode flow rate must be set based on the constraints of the application. For the application of the EDCS to life support systems discussed below, the cathode flow rate was set to achieve comparable CO_2 removal to commercial technologies. The cathode flow rate for HEMFC-powered vehicles was chosen based on the assumed stoichiometry of the stack.

Scaled EDCS Stack Projections

To compare the EDCS to incumbent technologies, a multi-cell 100 cm^2 stack using shorted membranes was designed. A diagram of the EDCS stack is shown in Fig. 5 and the important dimensions are included in Table II. A repeating unit in this module is a cathode frame and mesh, cathode, shorted membrane, anode, hydrogen diffusion barrier, anode frame and mesh. Then the same components in reverse: hydrogen diffusion barrier, anode, shorted membrane, and cathode to complete the repeating unit, followed by the next cathode frame and mesh. The 100 cm^2 active area was chosen to enable fabrication and lab-scale testing of the shorted module stack within the limitations of membrane casting and membrane electrode assembly preparation. Each cell within the stack is four times the size of single-cells tested previously. The size allows for reasonable scale-up and is relatively similar in size to the commercial 300 cm^2 fuel cells and electrolyzers.[68,69] Key concerns when scaling up is to ensure uniform flow distribution and low pressure drop. As such, a 2:1 aspect ratio for anode to cathode was chosen for the frames. The EDCS operates with an anode flow nearly 3 orders of magnitude lower than the cathode flow. The 2:1 aspect ratio provides a shorter, wider path for the much higher cathode flow to ensure uniform distribution and lower pressure drop. By using the shorted membrane rather than the standard AEM, bipolar plates can be eliminated from the stack. Additionally, the frames can be fabricated from engineered plastic rather than a conductive material, meaning they can be cheaper and lighter. The frames are sealed with gaskets against the membrane and contain the gas manifold which transports gas into and out of the mesh flow field. Without bipolar plates, the mesh of each frame is able to supply gas to the active area of two adjacent membranes, reducing the number of frames required. For example, in an 800 cm^2, 8-cell stack there would be 8 MEAs, 4 cathode frames, and 5 anode frames. Cathode frames must always be between two anode frames to ensure air flow is exposed to the cathode catalyst on both sides for adequate CO_2 capture and mass transport. The separator cells are sandwiched between two stainless steel end plates. The wet end plate supplies gas flow to the frame manifolds and provides a product flow path. The dry end plate ensures even sealing and compression of stack components.

The four areas of interest for investigating the use of the multi-cell EDCS stack are DAC, HEMFC vehicles, submarine life support, and space habitation. An operating paradigm was selected to minimize stack size while maximizing CO_2 flux and electron efficiency for each application. The operating conditions and resulting performance used as the basis for scaling calculations for each of the four applications are shown in Table III with steady-state CO_2 removal shown in the Supplemental Information (**Fig. SI-3**). Comparable CO_2 removal was selected to match incumbent technologies for a more direct comparison. As there are tradeoffs in the operating conditions and performance, some judgement was required to weigh the parameters based on the constraints of the application under review. The system parameters for each application and key experimental performance factors are shown in Tables IV, V, VI, and VII for DAC, HEMFCs, submarine, and space applications, respectively. A maximum stack size of approximately 350 cells was used.

The steady-state cell voltage was included for each application in **Fig. SI-3** to demonstrate the stability of the electrochemical device. Please note that upsets or instability at the beginning of the hold was due to non-steady operation as operating conditions were changed. Cell voltage is related to both the operating current density as well as the degree of carbonation within the cell. Higher current density or higher inlet CO_2 concentration resulted in lower cell voltage. It should be noted that operation at extremely low voltage did not negatively impact the stability of the outlet CO_2 concentration. Reduction in voltage over long-term operation (tens to hundreds of hours) indicates degradation of the electrochemical cell and will eventually negatively impact CO_2 removal performance; however, this is not the focus of the current work.

Version of record at: https://doi.org/10.1149/1945-7111/ac7adf

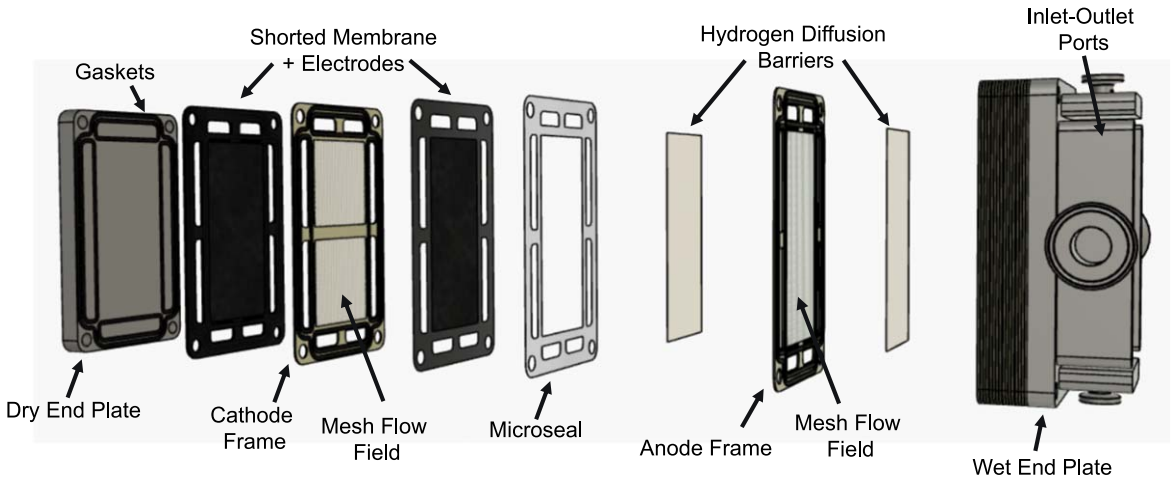

Figure 5. Exploded diagram of the building blocks of a proposed multi-cell, shorted-membrane EDCS stack with 100 cm^2 active area. The stack is composed of two end plates, plastic cathode frames, polypropylene mesh flow fields, and catalyst coated shorted membrane.

Table II. Multi-cell, 100 cm^2 EDCS stack dimensions.

End Plate	
Length	19.7 cm
Width	12.6 cm
Height	1.6 cm
Wet End Plate	682 cm^3
Dry End Plate	387 cm^3
Frame	
Length	19.7 cm
Width	12.6 cm
Height	0.12 cm
Active Area	
Length	14.1 cm
Width	7.1 cm
Anode Mesh Height	0.08 cm
Cathode Mesh Height	0.12 cm
Diffusion Barrier Height	0.02 cm
Cell Pitch	0.13 cm

electrolyzer and the EDCS as the reactions are reversed. Therefore, the addition of an EDCS will not impact the overall atom balance in life support systems. Using the water electrolyzer performance described in Li et al. (2020),[70] the size and load of the water electrolyzers needed for each of these applications was determined. For life support scenarios, the initial size of the water electrolyzer determined prior to the addition of the EDCS system. The results for the three applications are shown in Table VIII.

Direct air capture (DAC).—To remove 1 tonne per year from atmospheric air, a single 339-cell EDCS stack that is 7.7 L and weighs 17 kg will be required. The operating parameters were chosen for optimized CO_2 flux and electron efficiency while meeting a minimum CO_2 removal of 60%. As mentioned previously, hydrogen consumption and electron efficiency are the key factors to consider in DAC to ensure reasonable economics. As such, a low current density of 5 mA cm^{-2} was chosen as the basis for DAC scaling.

For comparison, Carbon Engineering has published a series of papers on their liquid amine CO_2 removal technology for DAC and the performance of their prototype.[10,71,72] At a slightly higher CO_2 removal rate of 74.5%, approximately 320 L of absorbent beds (excluding any additional volume associated with the regeneration equipment) would be required in order to remove 1 tonne per year of CO_2 based on the performance reported in Keith et al. (2018),[10] meaning the EDCS has the potential to be orders of magnitude more efficient on a volume basis.

Table III. Supporting 25 cm^2 single-cell performance data used in scaled EDCS stack calculations.

	DAC	HEMFC Vehicle		Submarine Life Support		Space Habitation	
Operating Temperature (°C)	40	60		60		40	
Inlet CO_2 Concentration (ppm)	400	400		5,000	3,000	3,000	2,000
Outlet CO_2 Concentration (ppm)	161	0.9	3.5	891	582	577	336
Current Density (mA cm^{-2})	5.0	35	45	50	50	45	45
Voltage (V)	0.458	0.335	0.273	0.033	0.051	0.034	0.008
Anode Flow (sccm H_2)	12	12	12	12	12	12	12
Cathode Flow (sccm Air + CO_2)	3000	2000	3300	2000	3000	2000	3000
Backpressure (anode-cathode, kPa(g))	0–0	150–150		0–0		0–0	

It is expected that the main cost contributor to EDCS operation and feasibility will be hydrogen consumption for DAC and both submarine and space life support systems. As such, preliminary analysis was performed to assess the impact of the EDCS on the power and size requirements of the upstream water electrolyzer in these systems. It is important to note that EDCS also consumes a small amount of oxygen from the air stream to produce the water byproduct, as seen in the electrochemical reactions shown in Eqs. 1 and 2 Based on the system stoichiometry, both hydrogen and oxygen will be supplied and consumed at the same rate between the water

Under the near ambient operating conditions chosen, the EDCS is estimated to consume 0.056 kg_{H_2}/kg_{CO_2}. The water electrolyzer necessary to supply H_2 to the EDCS for DAC is relatively small compared to the EDCS stack, only requiring 0.2% of the active area

Version of record at: https://doi.org/10.1149/1945-7111/ac7adf

Table IV. System requirements and EDCS stack design for DAC application, removing 1 tonne CO_2 per year from ambient air (400 ppm CO_2).

System Requirements—DAC	
System Basis	1 $tonne_{CO_2}$/yr
Feed Air CO_2 Concentration	400 ppm
EDCS Stack Design	
Temperature	40 °C
CO_2 Removal	60%
Air Flow	7.5 tonnes/day
H_2 Consumption	0.056 kg_{H_2}/kg_{CO_2}
Electron Efficiency	41%
CO_2 Flux	0.034 $kg_{CO_2}/m^2/h$
Required Active Area	3.4 m^2
Total Number of Cells	339
Stacks	1
Total EDCS Volume	7.7 L
Total EDCS Mass	17 kg

pressure drop are under consideration for further scale-up. An EDCS architecture with more open manifolds and/or thicker and more open mesh flow fields could potentially reduce pressure drop and operating costs per tonne of CO_2 removed.

Air treatment upstream of HEMFC in vehicles.—As mentioned previously, the HEMFC's performance is significantly reduced when the air feed contains CO_2 at ambient levels, and therefore CO_2 must be reduced in the incoming air to prevent this performance drop. The reported maximum acceptable CO_2 concentration in the incoming air fed to a HEMFC varies based on source, as does the acceptable power loss.[20,21,25,26,29,31,33,48–54] A full assessment of the sensitivity of HEMFCs to CO_2 is beyond the scope of this work. For a conservative estimate, the EDCS stack will target ⩾99% CO_2 removal to reduce the impact of air CO_2 on HEMFC performance. A 100 kW HEMFC stack operating with an air stoichiometry of 1.5 was used as the basis for evaluation of the EDCS in HEMFC vehicle applications. A target of less than 1 ppm CO_2 at the EDCS outlet (99.8% removal) would require two 351-cell EDCS stacks in parallel to process the HEMFC stack air supply. The required EDCS would be 17 L in volume and weigh 41 kg. For comparison, the PEMFC

Table V. System requirements for a 100-kW HEMFC stack with an EDCS upstream the air feed removing 99.8% and 99% of CO_2 from ambient air (400 ppm CO_2).

System Requirements—HEMFC Powered Vehicle			
System Basis		100 kW HEMFC Stack	
HEMFC Cell Peak Power Point		0.44 V at 1.4 A cm^{-2}	
HEMFC Air Stoichiometry	1.5		
Feed Air CO_2 Concentration		400 ppm	
Product Air CO_2 Concentration	<1 ppm		<4 ppm
Air Flow		430 kg h^{-1}	
EDCS Stack Design			
Temperature		60 °C	
CO_2 Removal	99.8%		99.0%
H_2 Consumption	0.33 kg_{H_2}/kg_{CO_2}		0.27 kg_{H_2}/kg_{CO_2}
Electron Efficiency	6.5%		8.3%
CO_2 Flux	0.039 $kg_{CO_2}/m^2/h$		0.064 $kg_{CO_2}/m^2/h$
Required Active Area	7.0 m^2		4.3 m^2
Total Number of Cells	702		426
Stacks	2		2
Total EDCS Volume	17 L		10 L
Total EDCS Mass	41 kg		26 kg

to generate the necessary H_2 to supply the EDCS stack. Minimizing hydrogen consumption is crucial for the EDCS to be feasible for commercialization as hydrogen adds to both the operating and capital costs. Therefore, a relatively high electron efficiency (in this case, 41%) was a key parameter in selecting the single-cell performance data. At the current renewable electrolytic hydrogen costs ranging from \$4–\$6,[73] the cost of removing one tonne of CO_2 would be \$223–335 when only accounting for hydrogen consumption. As of 2021, the U.S. Department of Energy has proposed the Hydrogen Shot initiative to reduce the cost of hydrogen to \$1/kg_{H_2} in the next decade.[74] If this cost target is met, the hydrogen cost of CO_2 removal by the EDCS would substantially reduce to \$56 per tonne CO_2. Future development may also reduce cost by increasing electron efficiency above the current value of 41%.

Another major contributor to the cost of removing CO_2 will be the energy to power fans or blowers as large amounts of air need to be treated in order to remove a substantial amount of atmospheric CO_2. This is beyond the scope of this work; however, the cost of the blower will likely be a significant portion of the total cost for the present design of our EDCS due to the pressure drop created by operating at such large air flow rates. Although an EDCS stack module was chosen for this work, other designs with ultra-low

stack in the Toyota Mirai only has a volume of around 37 L,[68] meaning if the HEMFC stack were of comparable size, the EDCS stack would add an additional 46% to the stack volume. However, the 1 ppm CO_2 outlet target may be too severe. Allowing a higher EDCS outlet concentration of up to 4 ppm (99% removal) reduces the EDCS stack volume to 10 L (two 213-cell stacks in parallel), corresponding to only 28% increase in system volume compared to the Toyota Mirai stack volume. Additionally, operation at 99% CO_2 removal is accompanied by 20% lower hydrogen consumption.

Further size reductions may be achieved by optimizing the stack geometry as the 100 cm^2 active cell area design may not be the most efficient for every application. Matching the active area to the 300 cm^2 Toyota Mirai stack could further reduce the volume of the EDCS stack, possibly by combining the end plates of both stacks or reducing the frame to active area ratio. Additionally, as the HEMFC technology is not commercialized at this point, it is possible there will be additional volume improvements based on enhanced cell performance that could ensure an overall system volume, including the EDCS, comparable to the PEMFC.

Hydrogen fuel cell stack systems typically operate with a recycle loop in order to maximize hydrogen utilization but require a small purge to offset nitrogen buildup due to crossover.[75] By using the

Version of record at: https://doi.org/10.1149/1945-7111/ac7adf

Table VI. System requirements and EDCS stack design for a 150-person crew in a submarine life support system, removing ~80% of CO_2 from cabin air containing 3000 and 5,000 ppm CO_2.

System Requirements—Submarine Life Support		
System Basis	150-person crew	
CO_2 Removal Rate	156 kg_{CO_2}/day	
Feed Air CO_2 Concentration	5,000 ppm	3,000 ppm
EDCS Stack Design		
Temperature	60 °C	
CO_2 Removal	82.2%	80.6%
Air Flow	25 tonne/day	42 tonne/day
H_2 Consumption	0.049 kg_{H_2} /kg_{CO_2}	0.056 kg_{H_2} /kg_{CO_2}
Electron Efficiency	47%	41%
CO_2 Flux	0.39 $kg_{CO_2}/m^2/h$	0.34 $kg_{CO_2}/m^2/h$
Required Active Area	16.9 m^2	19.2 m^2
Total Number of Cells	1687	1921
Stacks	5	6
Total EDCS Volume	38 L	44 L
Total EDCS Mass	85 kg	99 kg

Table VII. System requirements and EDCS stack design for a 6-person crew in space habitation, removing ~80% of CO_2 from cabin air containing 2000 and 3,000 ppm CO_2.

System Requirements—Space Habitation		
System Basis	6-person crew	
CO_2 Removal Rate	6.24 kg_{CO_2}/day	
Feed Air CO_2 Concentration	3,000 ppm	2,000 ppm
EDCS Stack Design		
Temperature	40 °C	
CO_2 Removal	81%	83%
Air Flow	1.1 tonne/day	1.7 tonne/day
H_2 Consumption	0.071 kg_{H_2} /kg_{CO_2}	0.073 kg_{H_2} /kg_{CO_2}
Electron Efficiency	32%	32%
CO_2 Flux	0.24 $kg_{CO_2}/m^2/h$	0.23 $kg_{CO_2}/m^2/h$
Required Active Area	1.1 m^2	1.2 m^2
Total Number of Cells	109	112
Stacks	1	1
Total EDCS Volume	3.2 L	3.3 L
Total EDCS Mass	10 kg	10 kg

purge as the hydrogen source for the EDCS rather than diverting fresh hydrogen, parasitic power consumption can be eliminated. The purge rate of the HEMFC stack is dependent on the purge control scheme and is in the range of 0.7%–1.2% of the hydrogen fed to the stack.[75,76] Based on the HEMFC stack design described and a hydrogen utilization of 0.99, the EDCS hydrogen consumption is 1.1% and 0.84% of the stack demand for the 99.9% and 99% CO_2 removal cases, respectively. This means that the hydrogen purge from the stack is viable option for the EDCS hydrogen source.

Submarine life support.—For the submarine life support system, a 150 person crew was used as the basis for the EDCS stack calculation. When maintaining a cabin CO_2 concentration of 5,000 ppm, an EDCS module containing five 338-cell, 100 cm^2 stacks in parallel with a total volume of 38 L and weighing 85 kg would be sufficient to handle crew respiration rates. The liquid amine system employed in submarines is nearly 1,800 L and weighs 2,270 kg.[17] The EDCS module is only 2.1% the size and 3.7% the weight of the LAS. Even when reducing the cabin CO_2 concentration down to 3,000 ppm, the EDCS is projected to be 44 L and weigh 99 kg, only 2.4% compared of LAS. The addition of an air blower and possible air pretreatment equipment such as a humidifier to the final EDCS module design will add to EDCS system volume. However, the bulk of the size and weight of the LAS is dedicated to the regeneration system and associated controls. Since the EDCS does not require external regeneration, a substantial fraction of the projected reduction in EDCS size compared to LAS will be realized upon final design. As such, the EDCS appears to be a promising technology for submarine life support systems based on the substantial reduction in size while providing improved air quality to the crew.

The addition of the EDCS in the submarine applications requires a 15 kW or 17 kW increase in electrolyzer power for the 5,000 ppm and 3,000 ppm CO_2 cases corresponding to a 45% and 51% increase in electrolyzer load, respectively. The increased electrolyzer load corresponds to 2.3 kWh/kg_{CO_2} and 2.7 kWh/kg_{CO_2} relative power consumption, respectively. It should be noted that the electrolyzer load increase in both submarine cases is less than the 26 kW power consumption of the liquid amine system, including thermal regeneration, pumping, etc.[17] This corresponds to 4.0 kWh/kg_{CO_2} for the liquid amine system, substantially higher than the projected power for CO_2 separation in the EDCS.

Manned-spacecraft air revitalization.—A 6-person crew in a manned spacecraft at 3,000 ppm CO_2 was used as the basis for space application. The basis accounts for 4 crewmembers plus the additional respiration rates of animals involved in onboard experiments.[63] A single 109-cell EDCS stack with a total volume of 3.2 L and weighing 10 kg would be sufficient to support a 6-person crew. The CDRA in operation on the ISS has a volume of 388 L and weighs 204 kg;[62] therefore, the EDCS is estimated to be less than 1% of the volume and less than 6% of the mass of the incumbent technology. Decreasing the target cabin air to 2,000 ppm

Table VIII. Calculated electrolyzer requirements to support EDCS systems in DAC and life support applications. EDCS performance shown in Tables IV, VI, and VII for submarine and space life support applications, respectively.

System	DAC	Submarine 150-person crew		Space 6-person crew	
Crew O_2 Consumption	—	135.5 kg_{O_2}/day		3.50 kg_{O_2}/day	
Base Electrolyzer Power	—	34 kW		1.4 kW	
Base Electrolyzer Active Area	—	0.70 m^2		0.028 m^2	
Feed Air CO_2 Concentration	400 ppm	5,000 ppm	3,000 ppm	3,000 ppm	2,000 ppm
EDCS O_2 Consumption	1.2 kg_{O_2}/day	60 kg_{O_2}/day	69 kg_{O_2}/day	3.5 kg_{O_2}/day	3.6 kg_{O_2}/day
Electrolyzer Power	0.30 kW	49 kW	51.3 kW	2.2 kW	2.3 kW
Electrolyzer Active Area	0.006 m^2	1.0 m^2	1.1 m^2	0.046 m^2	0.047 m^2
EDCS Energy Consumption	2.7 kWh/kg_{CO_2}	2.3 kWh/kg_{CO_2}	2.7 kWh/kg_{CO_2}	3.4 kWh/kg_{CO_2}	3.5 kWh/kg_{CO_2}

CO_2 results in a slight increase in EDCS size to 3.3 L weighing 10 kg. This is still less than 1% of the volume and only 4.8% of the weight of the CDRA. In the CDRA, the solid adsorbent beds are accompanied by a substantial footprint associated with the pressure-swing regeneration system and air pretreatment and post-treatment, meaning a significant portion of the equipment will not be required if replaced by the EDCS system.[77]

When both solid adsorbent beds in the CDRA are online (meaning no regeneration and no long-term operation), the CDRA can maintain a cabin air concentration of 3,000 ppm CO_2. In order to reach the lower CO_2 concentration target, the CDRA will require the addition of new beds and the associated controls or a substantial improvement in the adsorbent performance.[63] The scalability of the EDCS in stack form only results in a small increase in volume and weight when decreasing the target cabin air concentration from 3,000 ppm to 2,000 ppm. Further reductions in cabin air concentration or increases in crew size up to 19 crewmembers (at 3000 ppm) can be accomplished with the addition of more cells to the EDCS stack using the existing end plates.

For the manned spacecraft application, the electrolyzer power would increase by nearly 65% at both 2,000 ppm and 3,000 ppm CO_2 concentration cases. Although, it is important to note that the magnitude of power consumption in this system is low, on the order of 1 to 2 kW for the entire system. On a carbon dioxide removal basis, the power consumption in the manned spacecraft applications is 3.6 kWh/kg_{CO_2} and 3.5 kWh/kg_{CO_2} at inlet concentrations of 2,000 ppm and 3,000 ppm CO_2, respectively. For comparison, the CDRA consumes approximately 4.7 kWh/kg_{CO_2}.[78] The slightly higher power consumption in the space life support application relative to the submarine is due to operation at lower temperatures and CO_2 inlet concentrations, both of which reduce CO_2 flux and electron efficiency. However, the weight and volume constraints in the space application are more severe compared to the submarine system. As such, upstream temperature control equipment such as heat exchangers would be more detrimental to the EDCS design in the space life support system and have been avoided in the design process.

Conclusions

Interest in low concentration CO_2 removal technologies is on the rise. Here we have proposed and demonstrated the use of a compact and continuous electrochemically-driven CO_2 separator device for CO_2 removal from air at concentrations below 5,000 ppm. The EDCS was proposed for four different applications: direct air capture, air pretreatment for HEMFC vehicles, submarine life support, and space habitation. Based on the experimental data provided, the projected EDCS stack systems are feasible for DAC and more than met the CO_2 removal and size requirements in life support applications. Although the proposed stack design could be directly scaled and implemented in life support applications, for commercial application of DAC, a more open architecture may be required to decrease pressure drop to decrease the electrical operating costs associated with the fan or blower; however, there will be a tradeoff as these open architectures will likely result in an increase in gas-phase CO_2 mass transport resistance, leading to lower CO_2 removal performance. As the system is scaled, alternative designs will need be evaluated and a balance between pressure drop and CO_2 removal determined. In HEMFC vehicles, further improvement in the design is possible and may be required in order for the EDCS to be practical, especially when comparing the total system volume to the commercial PEMFC stacks available.

A 100 cm^2, multi-cell prototype EDCS is in the process of being fabricated to verify the projected EDCS stack performance and size calculations. Potential iterations of the EDCS design with larger active area may be pursued in order to optimize area to volume ratio which could benefit not only the HEMFC vehicle application but also DAC and the life support systems. Further work is also needed to fully define the EDCS system in life support applications to include any extraneous equipment such as air blowers, heat exchangers, or humidifiers to better compare to systems in operation. Once the full system design has been finalized for each application, a rigorous energy assessment and technoeconomic analysis can be used to further compare the EDCS to commercial CO_2 removal technologies.

Acknowledgments

The information, data, or work presented herein was funded in part by the Advanced Research Projects Agency-Energy (ARPA-E), U.S. Department of Energy, under Award Number DE-AR0001034. The views and opinions of authors expressed herein do not necessarily state or reflect those of the United States Government or any agency thereof.

Data Access Statement

The data that support the findings of this study are available in the online repository figshare at http://doi.org/10.6084/m9.figshare.20164013.

ORCID

Lin Shi https://orcid.org/0000-0001-5832-2238
Yun Zhao https://orcid.org/0000-0001-5531-7089
Shimshon Gottesfeld https://orcid.org/0000-0002-4391-5564
Brian P. Setzler https://orcid.org/0000-0001-7414-8372
Yushan Yan https://orcid.org/0000-0001-6616-4575

References

1. M. Sato and G. Schmidt, (2016), (https://data.giss.nasa.gov/modelforce/ghgases/).
2. National Oceanic and Atmospheric Administration, (2022), (https://gml.noaa.gov/ccgg/trends/global.html).
3. M. Fasihi, O. Efimova, and C. Breyer, *J. Clean. Prod.*, **224**, 957 (2019).
4. C. Zhao, Y. Guo, C. Li, and S. Lu, *Appl. Energy*, **124**, 241 (2014).
5. B. Li, Y. Duan, D. Luebke, and B. Morreale, *Appl. Energy*, **102**, 1439 (2013).
6. A. Gambhir and M. Tavoni, *One Earth*, **1**, 405 (2019).
7. K. S. Lackner, S. Brennan, J. M. Matter, A. H. Park, A. Wright, and B. van der Zwaan, *Proc Natl Acad Sci U S A*, **109**, 13156 (2012).
8. K. Z. House, A. C. Baclig, M. Ranjan, E. A. van Nierop, J. Wilcox, and H. J. Herzog, *Proc Natl Acad Sci U S A*, **108**, 20428 (2011).
9. M. Rahimi, G. Catalini, S. Hariharan, M. Wang, M. Puccini, and T. A. Hatton, *Cell Reports Physical Science*, **1**, 1 (2020).
10. D. W. Keith, G. Holmes, D. Angelo St., and K. Heidel, *Joule*, **2**, 1573 (2018).
11. S. Matz, B. P. Setzler, C. M. Weiss, L. Shi, S. Gottesfeld, and Y. Yan, *J. Electrochem. Soc.*, **168**, 014501 (2021).
12. L. Shi, Y. Zhao, S. Matz, S. Gottesfeld, B. P. Setzler, and Y. Yan, *Nature Energy*, **7**, 238 (2022).
13. R. J. Lowe, G. M. Huebner, and T. Oreszczyn, *Build. Serv. Eng. Res. Technol.*, **39**, 698 (2018).
14. D. Y. C. Leung, G. Caramanna, and M. M. Maroto-Valer, *Renew. Sustain. Energy Rev.*, **39**, 426 (2014).
15. J. Isobe, P. Henson, A. MacKnight, S. Yates, and D. Schuck, *46th International Conference on Environmental Systems," 1–10. ICES, Vienna, Austria* (2016), http://hdl.handle.net/2346/67727.
16. T. Shadle and T. Daley, *21st International Conference on Environmental Systems," San Francisco, California, USA* (1991).
17. R. Carey, A. Gomezplata, and A. Sarich, *Ocean Eng.*, **10**, 227 (1983).
18. Y. Zheng, G. Huang, M. Mandal, J. R. Varcoe, P. A. Kohl, and W. E. Mustain, *J. Electrochem. Soc.*, **168**, 024504 (2021).
19. X. Wang, W. Conway, R. Burns, N. McCann, and M. Maeder, *J. Phys. Chem.*, **114**, 1734 (2010).
20. N. Ziv, W. E. Mustain, and D. R. Dekel, *ChemSusChem*, **11**, 1136 (2018).
21. Y. Zheng, T. J. Omasta, X. Peng, L. Wang, J. R. Varcoe, B. S. Pivovar, and W. E. Mustain, *Energy Environ. Sci.*, **12**, 2806 (2019).
22. R. A. Wynveen, F. H. Schubert, and J. D. Powell, *One-Man, Self-Contained CO_2 Concentrating System Final Report, NASA* (1972) p.1–71https://ntrs.nasa.gov/citations/19720017484.
23. J. Winnick, R. D. Marshall, and F. H. Schubert, *Ind. Eng. Chem. Process Des. Dev.*, **13**, 59 (1974).
24. D. R. Dekel, *J. Power Sources*, **375**, 158 (2018).
25. M. Piana, M. Boccia, A. Filpi, E. Flammia, H. A. Miller, M. Orsini, F. Salusti, S. Santiccioli, F. Ciardelli, and A. Pucci, *J. Power Sources*, **195**, 5875 (2010).
26. M. Inaba, Y. Matsui, M. Saito, A. Tasaka, K. Fukuta, S. Watanabe, and H. Yanagi, *Electrochemistry*, **79**, 322 (2011).
27. G. Li et al., *Int. J. Hydrogen Energy*, **40**, 6655 (2015).
28. S. Suzuki, H. Muroyama, T. Matsui, and K. Eguchi, *Electrochim. Acta*, **88**, 552 (2013).
29. J. A. Wrubel, A. A. Peracchio, B. N. Cassenti, K. N. Grew, and W. K. S. Chiu, *J. Electrochem. Soc.*, **166**, F810 (2019).

30. J. A. Wrubel, A. A. Peracchio, B. N. Cassenti, T. D. Myles, K. N. Grew, and W. K. S. Chiu, *ECS Trans.*, **80**, 989 (2017).
31. T. Leyla, C. Nunes Kirchner, W. Germer, M. Zobel, and A. Dyck, *International Journal of Renewable Energy Development (IJRED)*, **3**, 65 (2014).
32. K. Fukuta, H. Inoue, S. Watanabe, and H. Yanagi, *ECS Trans.*, **19**, 23 (2009).
33. M. R. Gerhardt, L. M. Pant, and A. Z. Weber, *J. Electrochem. Soc.*, **166**, F3180 (2019).
34. B. Endrődi, E. Kecsenovity, A. Samu, T. Halmágyi, S. Rojas-Carbonell, L. Wang, Y. Yan, and C. Janáky, *Energy Environ. Sci.*, **13**, 4098 (2020).
35. J. Herranz, J. Durst, E. Fabbri, A. Patru, X. Cheng, A. A. Permyakova, and T. J. Schmidt, *Nano Energy*, **29**, 4 (2016).
36. J. Herranz, A. Patru, E. Fabbri, and T. J. Schmidt, *Current Opinion in Electrochemistry*, **23**, 89 (2020).
37. L.-C. Weng, A. T. Bell, and A. Z. Weber, *Energy Environ. Sci.*, **12**, 1950 (2019).
38. A. P. Muroyama, A. Pătru, and L. Gubler, *J. Electrochem. Soc.*, **167**, 133504 (2020).
39. M. D. Eisaman, D. E. Schwartz, S. Amic, D. Larner, J. Zesch, F. Torres, and K. Littau, "Energy-efficient electrochemical CO2 capture from the atmosphere." *Technical Proceedings of the 2009 Clean Technology Conference and Trade Show*, Houston, TX3-7 May p. 175–178 (2009).
40. J. Winnick, *Chem. Eng. Prog.*, **86**, 41 (1990).
41. K. Li and N. Li, *Sep. Sci. Technol.*, **28**, 1085 (1993).
42. S. Q. Xiao and K. W. Li, *Chem. Eng. Res. Des.*, **75**, 438 (1997).
43. J. Landon and J. R. Kitchin, *J. Electrochem. Soc.*, **157**, B1149 (2010).
44. H. W. Pennline, E. J. Granite, D. R. Luebke, J. R. Kitchin, J. Landon, and L. M. Weiland, *Fuel*, **89**, 1307 (2010).
45. W. A. Rigdon, T. J. Omasta, C. Lewis, M. A. Hickner, J. R. Varcoe, J. N. Renner, K. E. Ayers, and W. E. Mustain, *Journal of Electrochemical Energy Conversion and Storage*, **14**, 1 (2017).
46. A. P. Muroyama, A. Beard, B. Pribyl-Kranewitter, and L. Gubler, *ACS ES&T Engineering*, **1**, 905 (2021).
47. B. P. Setzler, Z. Zhuang, J. A. Wittkopf, and Y. Yan, *Nat. Nanotechnol.*, **11**, 1020 (2016).
48. Y. Zheng, G. Huang, L. Wang, J. R. Varcoe, P. A. Kohl, and W. E. Mustain, *J. Power Sources*, **467** (2020).
49. N. Ziv, A. N. Mondal, T. Weissbach, S. Holdcroft, and D. R. Dekel, *J. Membr. Sci.*, **586**, 140 (2019).
50. S. Gottesfeld, D. R. Dekel, M. Page, C. Bae, Y. Yan, P. Zelenay, and Y. S. Kim, *J. Power Sources*, **375**, 170 (2018).
51. T. Kimura and Y. Yamazaki, *Electrochemistry*, **79**, 94 (2011).
52. K. N. Grew, X. Ren, and D. Chu, *Electrochem. Solid-State Lett.*, **14**, B127 (2011).
53. U. Krewer, C. Weinzierl, N. Ziv, and D. R. Dekel, *Electrochim. Acta*, **263**, 433 (2018).
54. Z. Siroma, S. Watanabe, K. Yasuda, K. Fukuta, and H. Yanagi, *J. Electrochem. Soc.*, **158**, B682 (2011).
55. E. A. Ramskill, *SAE Trans.*, **70**, 350 (1962).
56. E. M. Mattox, J. C. Knox, and D. M. Bardot, *Acta Astronaut.*, **86**, 39 (2013).
57. W. Mazurek, *Submarine Air Monitoring and Purification International Symposium', Den Helder, The Netherlands, 5-8 October* (2015).
58. W. Raatschen, C. Matthias, and H. Westermann, *47th International Conference on Environmental Systems." ICES, Charleston, South Carolina, USA, 2017* (2017), http://hdl.handle.net/2346/72866.
59. T. A. Jacobson, J. S. Kler, M. T. Hernke, R. K. Braun, K. C. Meyer, and W. E. Funk, *Nature Sustainability*, **2**, 691 (2019).
60. C. Junaedi, K. Hawley, D. Walsh, S. Roychoudhury, S. Busby, M. B. Abney, J. L. Perry, and J. C. Knox, *"42nd International Conference on Environmental Systems," San Diego, California, USA* (2012), https://ntrs.nasa.gov/citations/20120015003.
61. E. Seedhouse, *Life Support System for Humans in Space* (Springer, Cham, Switzerland) (2020).
62. National Aeronautics and Space Administration, *NASA Technology Roadmaps TA 6: Human Health, Life Support, and Habitation Systems* (2015) p.1–217.
63. J. T. James, V. E. Meyers, W. Sipes, R. R. Scully, and C. M. Matty, *41st International Conference on Environmental Systems," Portland, Oregon, USA* (2011).
64. D. El Sherif and J. C. Knox, *35th International Conference on Environmental Systems." National Aeronautics and Space Administration, Rome, Italy* (2005).
65. S.-i Nakao, K. Yogo, K. Goto, T. Kai, and H. Yamada, *Advanced CO_2 Capture Technologies: Absorption, Adsorption, and Membrane Separation Methods* (Berlin) (Springer, Cham, Switzerland) (2019).
66. J. Wang et al., *Nat. Energy*, **4**, 392 (2019).
67. L. Shi, B. P. Setzler, K. Hu, C. M. Weiss, S. Matz, Y. Xue, Z. Xu, Z. Zhuang, S. Gottesfeld, and Y. Yan, *J. Electrochem. Soc.*, **167**, 144506 (2020).
68. T. Yoshida and K. Kojima, *The Electrochemical Society Interface*, **24**, 45 (2015).
69. Plug Power, *The Merrimack Electrolyzer Stack* (2020) p.1-2.
70. D. Li et al., *Nat. Energy*, **5**, 378 (2020).
71. G. Holmes and D. W. Keith, *Phil. Trans. R. Soc.*, **370**, 4380 (2012).
72. G. Holmes, K. Nold, T. Walsh, K. Heidel, M. A. Henderson, J. Ritchie, P. Klavins, A. Singh, and D. W. Keith, *Energy Procedia*, **37**, 6079 (2013).
73. J. Vickers, D. Peterson, and K. Randolph, *Cost of Electrolytic Hydrogen Production with Existing Technology* (Department of Energy, Record) 20004 (2020).
74. U. S. Department of Energy, (2021), Office of Energy Efficiency and Renewable Energyhttps://energy.gov/eere/fuelcells/hydrogen-shot.
75. R. K. Ahluwalia and X. Wang, *J. Power Sources*, **171**, 63 (2007).
76. A. Rabbani and M. Rokni, *Appl. Energy*, **111**, 1061 (2013).
77. J. C. Knox, *30th International Conference on Environmental Systems," Toulouse, France* (2000).
78. R. Kay, *Journal of Aerospace*, **107**, 514 (1998).